

Functional approach to the non-mesonic decay of Λ -hypernuclei

W. M. Alberico, A. De Pace, G. Garbarino

*Dipartimento di Fisica Teorica, Università di Torino
and INFN, Sezione di Torino, 10125 Torino, ITALY*

R. Cenni

*Dipartimento di Fisica dell'Università di Genova
and INFN, sezione di Genova, 33-16146 Genova, ITALY*
(April 26, 2024)

Abstract

We present an evaluation of the non-mesonic decay widths for Λ -hypernuclei ($\Lambda N \rightarrow NN$, $\Lambda NN \rightarrow NNN$) within the framework of the polarization propagator method. The full Λ self-energy is evaluated microscopically in nuclear matter by using the functional approach, which supplies a theoretically well grounded approximation scheme for the classification of the relevant diagrams, according to the prescriptions of the bosonic loop expansion. We employ average Fermi momenta, suitably adapted to different mass number regions (medium-light, medium and heavy hypernuclei). Moreover, we study the dependence of the decay rates on the NN and ΛN short range correlations. With a proper choice of the parameters which control these correlations in the new approximation scheme, it is possible to reproduce the experimental decay widths for $A \gtrsim 10$ hypernuclei.

21.80.+a, 13.75.Ev, 25.40.-h

I. INTRODUCTION

Among the existing hypernuclei, those which contain one Λ hyperon are the most stable with respect to the strong interaction and they are the subject of this paper. The study of hypernuclear physics is connected to various and general problems of both nuclear and particle physics. In fact, it helps in understanding important aspects of weak interactions in nuclei, the role of sub-nucleonic degrees of freedom in the hadron-hadron interactions and the renormalization properties of mesons and hyperons in the nuclear medium.

The most interesting hypernuclear decays are those involving weak processes, which directly concern the hyperon. The subject of the weak decay rates of hyperons embedded in nuclei has a quite long history, both on the theoretical and the experimental sides, but it has received a broader attention only in the last ten years. The weak decay of Λ -hypernuclei occurs through two different modes: the so called mesonic channel:

$$\Lambda \rightarrow \pi N \ (\Gamma_M), \quad (1.1)$$

and the non-mesonic one, which can be mainly attributed to the following processes:

$$\Lambda N \rightarrow NN \ (\Gamma_1), \quad (1.2)$$

$$\Lambda NN \rightarrow NNN \ (\Gamma_2), \quad (1.3)$$

both mediated by the exchange of $\pi, \rho, \eta, \omega, K, K^*$, etc. The non-mesonic mode is only possible in nuclear systems and, nowadays, due to the difficulty of using Λ beams, the study of the Λ decay in nuclei is the only way to get information on the weak process $\Lambda N \rightarrow NN$.

The free Λ decay is compatible with the $\Delta I = 1/2$ isospin rule, which is based on the observed ratio $\Gamma_{\Lambda \rightarrow \pi^- p} / \Gamma_{\Lambda \rightarrow \pi^0 n} \simeq 2$, but it is not yet understood on theoretical grounds. Besides, because of nuclear shell effects, it is not yet clear the level of violation of this rule for the mesonic decay in nuclear systems. In the present calculation we will assume this rule as valid. The momentum of the outgoing nucleon in the process $\Lambda \rightarrow \pi N$ is about 100 MeV, hence this decay mode is suppressed by the Pauli principle in nuclei, particularly in heavy systems (in infinite nuclear matter being strictly forbidden): the mesonic width is found to decrease fast as the mass number A of the hypernucleus increases [1–3]. This is confirmed by the few available experimental data.

In the non-mesonic process $\Lambda N \rightarrow NN$, the final nucleons have large momenta ($\simeq 420$ MeV) and, apart from the s -shell hypernuclei, it dominates over the mesonic decay. The presence of large momentum transfers in the non-mesonic channels implies that the details of the nuclear structure have only little influence on the decay, but, on the other hand, the NN and ΛN short range correlations are crucial. There appears to be an anticorrelation between mesonic and non-mesonic decay, such that the total width is quite stable from light to heavy hypernuclei. In fact, as discussed in ref. [1], the non-mesonic rates Γ_1

and Γ_2 increase and reach saturation values as the mass number of the nucleus increases: $\Gamma_{NM}(\Lambda^{208}\text{Pb})/\Gamma_{NM}(\Lambda^{12}\text{C}) \simeq 1.4$, where $\Gamma_{NM} = \Gamma_1 + \Gamma_2$.

In this paper we present an evaluation of the decay rates for a Λ in nuclear matter within the framework of the polarization propagators. The relevant Feynman diagrams have been obtained following a functional approach, which allows to divide these diagrams into classes, according to the prescription of the so-called bosonic loop expansion (BLE). The calculation in finite nuclei (using the local density approximation) is not possible here because of the long computing time already for the calculation of the decay widths at fixed Fermi momentum (namely in nuclear matter). Nevertheless, in order to consider different mass regions, we assign an average Fermi momentum felt by the hyperon in the various nuclei.

We remind that the baryon-baryon strong interactions cannot be treated with the standard perturbative method. However, in the study of nuclear phenomena we always need to sum up the relevant diagrams. For instance, one usually performs the summation of the infinite classes of diagrams entailed by the RPA and Hartree-Fock approximations. However, in the above quoted schemes no prescription is given to evaluate the “next-to-leading” order.

The functional techniques can provide a theoretically founded derivation of new classes of expansion in terms of powers of suitably chosen parameters. On the other hand, as we will see, the RPA automatically appears in this framework as the mean field level. The method has been extensively applied to different processes in nuclear physics [4–6]. We will use it for the calculation of the Λ decay rates in nuclear matter, which can be expressed through the nuclear responses to pseudoscalar-isovector and vector-isovector fields. We will see that the responses include ring-dressed meson propagators (which represent the mean field level of the theory) and almost the whole spectrum of $2p-2h$ excitations (expressed in terms of a one-loop expansion with respect to the ring-dressed meson propagators) which are required for the evaluation of Γ_2 . Actually, the semiclassical expansion leads to the prescription of grouping the relevant Feynman diagrams in a consistent many-body description of the “in medium” meson self-energies: the general theorems and sum rules of the theory are preserved.

The paper is organized as follows. In Sec. II we summarize the model used for the calculation of the decay rates. In Sec. III the functional approach to the spin-isospin nuclear response functions is presented. By using the semiclassical approximation we will introduce the class of Feynman diagrams needed for the evaluation of Γ_2 . Our results are presented and discussed in Sec. IV: we first study the sensitivity of the decay rates to the NN and ΛN short range correlations, and then we parametrize these correlations in order to reproduce the experimental decay widths for three different mass regions in the hypernuclear spectrum. Our conclusions are given in Sec. V.

II. POLARIZATION PROPAGATOR METHOD

In this section we briefly summarize how the Λ decay in nuclear matter can be studied employing the polarization propagator method [7,8,1]. This technique provides a unified picture of the different decay channels and it is equivalent to the standard wave function method, used by other authors in refs. [2,9–11,3]. In a previous work [1] the evaluation of the decay widths was first performed in nuclear matter and then extended to finite nuclei via the local density approximation: in this framework the experimental partial decay rates in a range of nuclei from $^{12}\Lambda\text{C}$ to $^{208}\Lambda\text{Pb}$ have been reproduced. The two-body induced decay $\Lambda NN \rightarrow NNN$ has been accounted for via a purely phenomenological parametrization (using data on pionic atoms) of the $2p$ - $2h$ polarization propagator which enters the Λ self-energy Σ_Λ . The total decay rate is obtained through the relation:

$$\Gamma_\Lambda = -2\text{Im}\Sigma_\Lambda. \quad (2.1)$$

Here we present a microscopic calculation of the $2p$ - $2h$ polarization propagator within the theoretically consistent scheme which will be introduced in the next section.

Let us first remind the main steps in the evaluation of Γ_Λ . We start from the $\Lambda \rightarrow \pi N$ effective lagrangian:

$$\mathcal{L}_{\Lambda\pi N} = Gm_\pi^2\bar{\psi}_N(A + B\gamma_5)\boldsymbol{\tau} \cdot \boldsymbol{\phi}_\pi\psi_\Lambda + h.c., \quad (2.2)$$

where the values of the weak coupling constants $G \simeq 2.211 \cdot 10^{-7}/m_\pi^2$, $A = 1.06$, $B = -7.10$ are fixed from the free Λ decay. The constants A and B determine the strengths of the parity violating and parity conserving $\Lambda \rightarrow \pi N$ amplitudes, respectively. In order to enforce the $\Delta I = 1/2$ rule, in eq. (2.2) the hyperon is assumed to be an isospin spurion with $I_z = -1/2$. Using the Feynman rules, in the non relativistic limit the Λ self-energy in nuclear matter is (see fig. 1):

$$\Sigma_\Lambda(k) = 3i(Gm_\pi^2)^2 \int \frac{d^4q}{(2\pi)^4} \left\{ S^2 + \frac{P^2}{m_\pi^2} \mathbf{q}^2 \right\} F_\pi^2(q) G_N(k-q) G_\pi(q). \quad (2.3)$$

Here, $S = A$, $P = m_\pi B/2m_N$, while:

$$G_N(p) = \frac{\theta(|\mathbf{p}| - k_F)}{p_0 - E_N(\mathbf{p}) - V_N + i\epsilon} + \frac{\theta(k_F - |\mathbf{p}|)}{p_0 - E_N(\mathbf{p}) - V_N - i\epsilon}, \quad (2.4)$$

and:

$$G_\pi(q) = \frac{1}{q_0^2 - \mathbf{q}^2 - m_\pi^2 - \Sigma_\pi^*(q)}, \quad (2.5)$$

are the nucleon and pion propagators in nuclear matter, respectively. In the above, $p = (p_0, \mathbf{p})$ and $q = (q_0, \mathbf{q})$ denote four-vectors, k_F is the Fermi momentum, E_N is the nucleon total free energy, V_N is the nucleon binding energy (assumed constant), and Σ_π^* is the pion

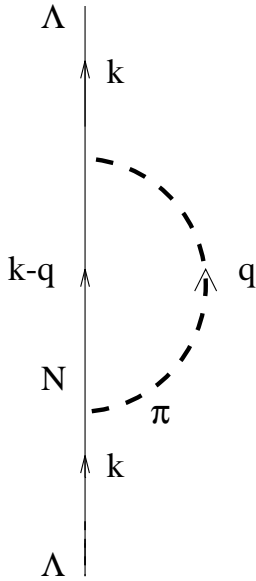


FIG. 1. Λ self energy in nuclear matter (the dashed line represents a dressed pion).

proper self-energy. Moreover, in eq. (2.3) we have included a monopole form factor for the $\pi\Lambda N$ vertex:

$$F_\pi(q) = \frac{\Lambda_\pi^2 - m_\pi^2}{\Lambda_\pi^2 - q_0^2 + \mathbf{q}^2}, \quad (2.6)$$

with the same cut-off $\Lambda_\pi = 1.3$ GeV used for the πNN strong vertex. In fig. 2 we explicitly show the lowest order Feynman graphs for the Λ self-energy. Diagram (a) represents the bare self-energy term, including the effects of Pauli principle and of the binding on the intermediate nucleon. In (b) and (c) the pion couples to a particle-hole (p - h) and a Δ - h pairs, respectively. In diagrams (d) and (e) we show examples of $2p$ - $2h$ excitations, while (f) is a RPA iteration of diagram (b). Once evaluated the integral over q_0 in (2.3), the nuclear matter Λ decay width (eq. (2.1)) becomes [7]:

$$\Gamma_\Lambda(\mathbf{k}, \rho) = -6(Gm_\pi^2)^2 \int \frac{d\mathbf{q}}{(2\pi)^3} \theta(|\mathbf{k} - \mathbf{q}| - k_F) \theta(k_0 - E_N(\mathbf{k} - \mathbf{q}) - V_N) \times \text{Im} \alpha(q) \Big|_{q_0=k_0-E_N(\mathbf{k}-\mathbf{q})-V_N}, \quad (2.7)$$

where

$$\begin{aligned} \alpha(q) = & \left\{ S^2 + \frac{P^2}{m_\pi^2} \mathbf{q}^2 \right\} F_\pi^2(q) G_\pi^0(q) + \frac{\tilde{S}^2(q) U_L(q)}{1 - V_L(q) U_L(q)} \\ & + \frac{\tilde{P}_L^2(q) U_L(q)}{1 - V_L(q) U_L(q)} + \frac{\tilde{P}_T^2(q) U_T(q)}{1 - V_T(q) U_T(q)}, \end{aligned} \quad (2.8)$$

consist of a longitudinal and a transverse part. In eq. (2.7) the first θ -function forbids intermediate nucleon momenta (see fig. 1) smaller than the Fermi momentum and the second

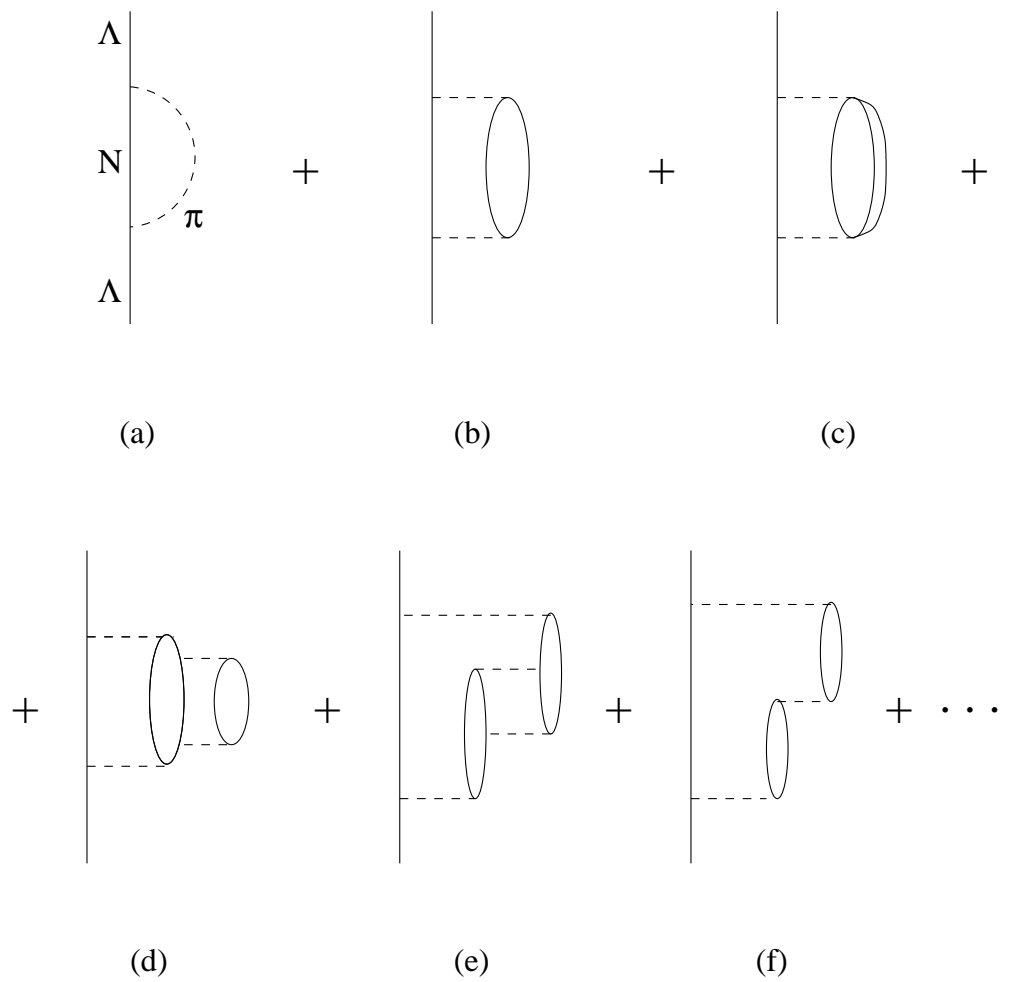


FIG. 2. Lowest order terms for the Λ self-energy in nuclear matter. The meaning of the various diagramms is explained in the text.

one requires the pion energy q_0 to be positive. Moreover, the Λ energy, $k_0 = E_\Lambda(\mathbf{k}) + V_\Lambda$, contains a binding term. The pion lines of fig. 2 have been replaced in eq. (2.8) by the interactions V_L , V_T , \tilde{S} , \tilde{P}_L , \tilde{P}_T , which include π and ρ exchange modulated by the effect of short range correlations. They have the following expressions:

$$V_L(q) = \frac{f_\pi^2}{m_\pi^2} \left\{ \mathbf{q}^2 F_\pi^2(q) G_\pi^0(q) + g_L(q) \right\}, \quad (2.9)$$

$$V_T(q) = \frac{f_\pi^2}{m_\pi^2} \left\{ \mathbf{q}^2 C_\rho F_\rho^2(q) G_\rho^0(q) + g_T(q) \right\}. \quad (2.10)$$

$$\tilde{P}_L(q) = \frac{f_\pi}{m_\pi} \frac{P}{m_\pi} \left\{ \mathbf{q}^2 F_\pi^2(q) G_\pi^0(q) + g_L^\Lambda(q) \right\}, \quad (2.11)$$

$$\tilde{P}_T(q) = \frac{f_\pi}{m_\pi} \frac{P}{m_\pi} g_T^\Lambda(q), \quad (2.12)$$

$$\tilde{S}(q) = \frac{f_\pi}{m_\pi} S \left\{ F_\pi^2(q) G_\pi^0(q) - \tilde{F}_\pi^2(q) \tilde{G}_\pi^0(q) \right\} |\mathbf{q}|. \quad (2.13)$$

In the above, $G_M^0 = 1/(q_0^2 - \mathbf{q}^2 - m_M^2)$ denotes a free meson propagator and F_ρ is the ρNN form factor (eq. (2.6) with cut-off $\Lambda_\rho = 2.5$ GeV). The exchange of ρ -mesons is brought into play by the short range correlation \tilde{P}_T embodied in the $\Lambda N \rightarrow NN$ potential. Form factors and propagators with a tilde imply that they are calculated with the replacement $\mathbf{q}^2 \rightarrow \mathbf{q}^2 + q_c^2$, where $1/q_c$ is a lenght of the order of the hard core radius of the interaction, and C_ρ is the ratio:

$$C_\rho = \frac{f_\rho^2}{m_\rho^2} \left[\frac{f_\pi^2}{m_\pi^2} \right]^{-1}. \quad (2.14)$$

The short range correlations included in the potentials of eqs. (2.9)-(2.12) are explicitly reported in the appendix of ref. [1]. Their momentum dependence (governed by the parameter q_c) ensures the convergence of the integrals contained in diagrams like (d) and (e) of fig. 2 (this behaviour is not crucial in ring approximation). In the calculation, the values of the correlation functions in $q = 0$,

$$g' \equiv g_{L,T}(0), \quad g'_\Lambda \equiv g_{L,T}^\Lambda(0) \quad (2.15)$$

(namely the Landau parameters), will be considered as free.

Furthermore, in eq. (2.8) U_L and U_T contain the Lindhard functions for p - h and Δ - h excitations [12] and also account for the irriducible $2p$ - $2h$ polarization propagator:

$$U_{L,T}(q) = U^{ph}(q) + U^{\Delta h}(q) + U_{L,T}^{2p2h}(q). \quad (2.16)$$

They appear in eq. (2.8) within the standard RPA expression. The Lindhard functions U^{ph} , $U^{\Delta h}$ are normalized as in ref. [13]. In the following section we will develop an approximation scheme for the classification of the various diagrams to be included in the calculation of the Λ self-energy. Eq. (2.7) depends, both explicitly and through $U_{L,T}(q)$, on the nuclear matter density $\rho = 2k_F^3/3\pi^2$.

We remind that in nuclear matter the mesonic decay is strictly forbidden, the final nucleon in $\Lambda \rightarrow \pi N$ having a momentum lower than the Fermi one (for a Λ decaying at rest, $q \simeq 100$ MeV $< k_F \simeq 270$ MeV). In finite nuclei the mesonic rate is dominant only in s -shell hypernuclei and rapidly decreases with the mass number.

III. FUNCTIONAL APPROACH TO THE SPIN-ISOSPIN NUCLEAR RESPONSE FUNCTIONS

We first evaluate the polarization propagator in the pionic (spin-longitudinal) channel. In order to exemplify we consider a lagrangian describing a system of nucleons interacting with pions through a pseudoscalar coupling:

$$\mathcal{L}_{\pi N} = \bar{\psi}(i\partial - m_N)\psi + \frac{1}{2}\partial_\mu\phi \cdot \partial^\mu\phi - \frac{1}{2}m_\pi^2\phi^2 - i\bar{\psi}\Gamma\psi \cdot \phi, \quad (3.1)$$

where ψ (ϕ) is the nucleonic (pionic) field, and:

$$\Gamma = g\gamma_5\tau \quad (3.2)$$

($g = 2f_\pi m_N/m_\pi$) is the spin-isospin matrix in the spin-longitudinal isovector channel. We remind that in the calculation of the hypernuclear decay rates we also need the polarization propagator in the transverse channel (see eqs. (2.7),(2.8)): hence, we will have to include in the model another mesonic degree of freedom, the ρ meson. As we will see, the semiclassical expansion is characterized by the topology of the diagrams, so the same scheme can be applied to mesonic fields other than the pionic one. In this section we use a relativistic formalism, the non-relativistic reduction of our results being trivial.

Let us now introduce a *classical* external field φ with the quantum numbers of the pion. The lagrangian then becomes:

$$\mathcal{L}_{\pi N} \rightarrow \mathcal{L}_{\pi N} - i\bar{\psi}\Gamma\psi \cdot \varphi. \quad (3.3)$$

The corresponding generating functional in terms of Feynman path integrals has the form:

$$Z[\varphi] = \int \mathcal{D}[\bar{\psi}, \psi, \phi] \exp \left\{ i \int dx [\mathcal{L}_{\pi N}(x) - i\bar{\psi}(x)\Gamma\psi(x) \cdot \varphi(x)] \right\} \quad (3.4)$$

(here and in the following the coordinate integrals are 4-dimensional). All the fields in the functional integrals have to be considered as classical variables, but with the correct commuting properties. The physical quantities of interest for the problem are deduced from

the generating functional by means of functional differentiations. By introducing a new functional Z_c such that

$$Z[\boldsymbol{\varphi}] = \exp \{iZ_c[\boldsymbol{\varphi}]\}, \quad (3.5)$$

the polarization propagator turn out to be the second functional derivative of Z_c with respect to the source $\boldsymbol{\varphi}$ of the pionic field:

$$\Pi_{ij}(x, y) = - \left[\frac{\delta^2 Z_c[\boldsymbol{\varphi}]}{\delta \varphi_i(x) \delta \varphi_j(y)} \right]_{\boldsymbol{\varphi}=0}. \quad (3.6)$$

We notice that the use of Z_c instead of Z in eq. (3.6) amounts to cancel the disconnected diagrams of the perturbative expansion (linked cluster theorem). From the generating functional Z one can obtain different approximation schemes according to the order in which the functional integrations are performed. By integrating eq. (3.4) over the mesonic degrees of freedom *first*, the generating functional can be written in terms of a fermionic effective action S_{eff}^F . Up to an irrelevant multiplicative constant:

$$Z[\boldsymbol{\varphi}] = \int \mathcal{D}[\bar{\psi}, \psi] \exp \left\{ iS_{\text{eff}}^F[\bar{\psi}, \psi] \right\}. \quad (3.7)$$

The remaining integration variables are interpreted as physical fields and S_{eff}^F describes a quadrilinear non-local time- or energy-dependent nucleon-nucleon interaction induced by the exchange of one pion:

$$\begin{aligned} S_{\text{eff}}^F[\bar{\psi}, \psi] = & \int dx dy \left[\bar{\psi}(x) G_N^{-1}(x-y) \psi(y) \right. \\ & \left. + \frac{1}{2} \sum_{i=1}^3 \bar{\psi}(x) \Gamma_i \psi(x) G_\pi^0(x-y) \bar{\psi}(y) \Gamma_i \psi(y) \right], \end{aligned} \quad (3.8)$$

where G_N and G_π^0 are the nucleon and free pion propagators, respectively, which satisfy the following field equations:

$$(i\partial_x - m_N - i\boldsymbol{\Gamma} \cdot \boldsymbol{\varphi}) G_N(x-y) = \delta(x-y), \quad (3.9)$$

$$(\square_x + m_\pi^2) G_\pi^0(x-y) = -\delta(x-y). \quad (3.10)$$

The pion propagator is diagonal in the isospin indices: $(G_\pi^0)_{ij} = \delta_{ij} G_\pi^0$. The effective action (3.8) can then be utilized in the framework of ordinary perturbation theory and will not be employed in the following. In fact, it does not bring significant novelties with respect to the usual calculations; furthermore, it cannot be correctly renormalized due to the absence of a term proportional to ϕ^4 , which is needed to cancel the divergence of the 4-points fermion loops.

A. The bosonic effective action

Alternatively, it is possible to eliminate in eq. (3.4) the nucleonic degrees of freedom first (without destroying the renormalizability of the theory [5]). Introducing the change of variable $\phi \rightarrow \phi - \varphi$, eq. (3.4) becomes:

$$\begin{aligned} Z[\varphi] &= \exp \left\{ \frac{i}{2} \int dx dy \varphi(x) \cdot G_\pi^{0^{-1}}(x-y) \varphi(y) \right\} \\ &\quad \times \int \mathcal{D} [\bar{\psi}, \psi, \phi] \exp \left\{ i \int dx dy [\bar{\psi}(x) G_N^{-1}(x-y) \psi(y) \right. \\ &\quad \left. + \frac{1}{2} \phi(x) \cdot G_\pi^{0^{-1}}(x-y) (\phi(y) + 2\varphi(y))] \right\}, \end{aligned} \quad (3.11)$$

where the integral over $[\bar{\psi}, \psi]$ is gaussian:

$$\int \mathcal{D} [\bar{\psi}, \psi] \exp \left\{ i \int dx dy \bar{\psi}(x) G_N^{-1}(x-y) \psi(y) \right\} = (\det G_N)^{-1}. \quad (3.12)$$

Hence, multiplying eq. (3.11) by the unessential factor $\det G_N^0$ (G_N^0 being the free nucleon propagator), which only redefines the normalization constant of the generating functional, and using the property $\det X = \exp \{ \text{Tr} \ln X \}$, we obtain:

$$Z[\varphi] = \exp \left\{ \frac{i}{2} \int dx dy \varphi(x) \cdot G_\pi^{0^{-1}}(x-y) \varphi(y) \right\} \int \mathcal{D} [\phi] \exp \left\{ i S_{\text{eff}}^B [\phi] \right\}, \quad (3.13)$$

with:

$$S_{\text{eff}}^B [\phi] = \int dx dy \left\{ \frac{1}{2} \phi(x) \cdot G_\pi^{0^{-1}}(x-y) [\phi(y) + 2\varphi(y)] + V_\pi[\phi] \right\}, \quad (3.14)$$

$$\begin{aligned} V_\pi[\phi] &= i \text{Tr} \sum_{n=1}^{\infty} \frac{1}{n} (i\Gamma \cdot \phi G_N^0)^n \\ &= \frac{1}{2} \sum_{i,j} \text{Tr} (\Gamma_i \Gamma_j) \int dx dy \Pi^0(x, y) \phi_i(x) \phi_j(y) \\ &\quad + \frac{1}{3} \sum_{i,j,k} \text{Tr} (\Gamma_i \Gamma_j \Gamma_k) \int dx dy dz \Pi^0(x, y, z) \phi_i(x) \phi_j(y) \phi_k(z) + \mathcal{O}(\phi^4), \end{aligned} \quad (3.15)$$

where

$$-i\Pi^0(x, y) = iG_N^0(x-y) iG_N^0(y-x), \quad (3.16)$$

$$-i\Pi^0(x, y, z) = iG_N^0(x-y) iG_N^0(y-z) iG_N^0(z-x), \quad \text{etc.} \quad (3.17)$$

We have thus derived an effective action for the bosonic field ϕ . This action contains a term for the free pion field and also a highly non-local pion self-interaction V_π , which is described by the Feynman diagrams shown in fig. 3. This effective interaction is given by the sum of all the diagrams containing one closed fermion loop. We note that the function of eq. (3.16) is the free polarization propagator, namely the Lindhard function. Moreover, the functions $\Pi^0(x, y, \dots, z)$ are symmetric for cyclic permutations of the arguments.

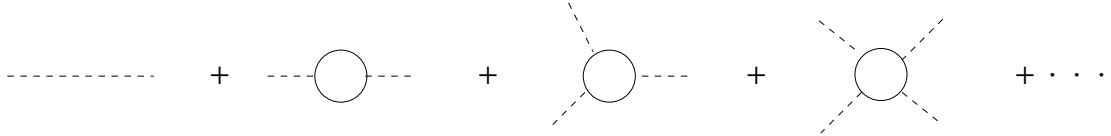


FIG. 3. Diagrammatic representation of the bosonic effective action (3.14).

B. Semiclassical expansion

The next step is the evaluation of the functional integral over the bosonic degrees of freedom in eq. (3.13). A perturbative approach to the bosonic effective action (3.14) does not seem to provide any valuable results within the capabilities of the present computing tools and we will use here another approximation scheme, namely the semiclassical method.

Mean field level

The lowest order of the semiclassical expansion is the stationary phase approximation (also called saddle point approximation (SPA) in the euclidean space): we require the bosonic effective action to be stationary with respect to arbitrary variations of the fields ϕ_i :

$$\frac{\delta S_{\text{eff}}^B[\phi]}{\delta \phi_i(x)} = 0. \quad (3.18)$$

From the partial derivative of eq. (3.14) we obtain for the classical field ϕ the following equation of motion:

$$(\square + m_\pi^2) \phi_i(x) = \int dy G_\pi^{0^{-1}}(x-y) \varphi_i(y) + \frac{\delta V_\pi[\phi]}{\delta \phi_i(x)}, \quad (3.19)$$

whose solutions are functional of the external source φ . The exact solution cannot be written down explicitly. However, due to the particular form of $V_\pi[\phi]$, when $\varphi \rightarrow 0$, one solution is $\phi = 0$; we can then express the general solution of eq. (3.19) as an expansion in powers of φ :

$$\phi_i^0(x) = \sum_j \int dy A_{ij}(x, y) \varphi_j(y) + \frac{1}{2} \sum_{j, k} \int dy dz B_{ijk}(x, y, z) \varphi_j(y) \varphi_k(z) + \mathcal{O}(\varphi^3). \quad (3.20)$$

Substituting eqs. (3.20) and (3.15) into (3.19) and keeping the terms linear in φ_i we obtain the following relation for A_{ij} :

$$A_{ij}(x, y) - \text{Tr}(\Gamma_i^2) \int du dv G_\pi^0(x-u) \Pi^0(u, v) A_{ij}(v, y) = \delta_{ij} \delta(x-y). \quad (3.21)$$

Finally, by introducing the ring-dressed pion propagator G_π^{ring} , which satisfies the Dyson equation:

$$G_\pi^{\text{ring}}(x-y) = G_\pi^0(x-y) + \text{Tr}(\Gamma_i^2) \int du dv G_\pi^0(x-u) \Pi^0(u, v) G_\pi^{\text{ring}}(v-y), \quad (3.22)$$

or, formally:

$$G_\pi^{\text{ring}} = \frac{G_\pi^0}{1 - \text{Tr}(\Gamma_i^2) G_\pi^0 \Pi^0}, \quad (3.23)$$

the solution of (3.21) reads:

$$A_{ij}(x, y) = \delta_{ij} \int dz G_\pi^{\text{ring}}(x-z) G_\pi^{0^{-1}}(z-y). \quad (3.24)$$

Therefore, the saddle point of (3.14) at first order in the source φ is:

$$\phi_i^{\text{ring}}(x) = \int dy dz G_\pi^{\text{ring}}(x-z) G_\pi^{0^{-1}}(z-y) \varphi_i(y) \equiv \int dy (G_\pi^{\text{ring}} G_\pi^{0^{-1}})(x-y) \varphi_i(y), \quad (3.25)$$

and the corresponding bosonic effective action reads:

$$S_{\text{eff}}^B [\phi^{\text{ring}}] = -\frac{1}{2} \int dx dy du dv G_\pi^{0^{-1}}(x-u) \varphi(u) \cdot G_\pi^{\text{ring}}(x-y) G_\pi^{0^{-1}}(y-v) \varphi(v). \quad (3.26)$$

Now, the generating functional of eq. (3.13) takes the form:

$$\begin{aligned} Z[\varphi] = & \exp \left\{ \frac{i}{2} \int dx dy du dv \varphi(u) \cdot G_\pi^{0^{-1}}(x-u) \right. \\ & \times \left. [G_\pi^0(x-y) - G_\pi^{\text{ring}}(x-y)] G_\pi^{0^{-1}}(y-v) \varphi(v) \right\}. \end{aligned} \quad (3.27)$$

The polarization propagator is then evaluated using eqs. (3.5), (3.6). We obtain that in the saddle point approximation it coincides with the well known ring expression:

$$\begin{aligned} \Pi_{ij}(x, y) = & \delta_{ij} \left[\Pi^0(x, y) + \text{Tr}(\Gamma_i^2) \int du dv \Pi^0(x, u) G_\pi^{\text{ring}}(u-v) \Pi^0(v, y) \right] \\ \equiv & \delta_{ij} \Pi^{\text{ring}}(x, y), \end{aligned} \quad (3.28)$$

or, formally:

$$\Pi = \frac{\Pi^0}{1 - \text{Tr}(\Gamma_i^2) G_\pi^0 \Pi^0} \equiv \Pi^{\text{ring}}. \quad (3.29)$$

Hence, the ring approximation corresponds to the mean field level of the present effective theory.

Quantum fluctuations around the mean field solution (one-loop corrections)

In the next step of our semiclassical expansion we write the bosonic effective action as:

$$S_{\text{eff}}^B [\phi] = S_{\text{eff}}^B [\phi^0] + \frac{1}{2} \sum_{ij} \int dx dy \left[\frac{\delta^2 S_{\text{eff}}^B [\phi]}{\delta \phi_i(x) \delta \phi_j(y)} \right]_{\phi=\phi^0} [\phi_i(x) - \phi_i^0(x)] [\phi_j(y) - \phi_j^0(y)], \quad (3.30)$$

where now ϕ^0 also contains the second order term in the source φ (see eq (3.20)). Then, after performing the gaussian integration over ϕ , the generating functional reads:

$$Z[\varphi] = \exp \left\{ \frac{i}{2} \int dx dy \varphi(x) \cdot G_\pi^{0^{-1}}(x-y) \varphi(y) \right\} \times \exp \left\{ iS_{\text{eff}}^B[\phi^0] - \frac{1}{2} \text{Tr} \ln \left[\frac{\delta^2 S_{\text{eff}}^B[\phi]}{\delta \phi_i(x) \delta \phi_j(y)} \right]_{\phi=\phi^0} \right\}, \quad (3.31)$$

and the polarization propagator is:

$$\Pi_{ij}(x, y) = - \left\{ \frac{\delta^2}{\delta \varphi_i(x) \delta \varphi_j(y)} \left[S_{\text{eff}}^B[\phi^0] + \frac{i}{2} \text{Tr} \ln \left(\frac{\delta^2 S_{\text{eff}}^B[\phi]}{\delta \phi_k(x) \delta \phi_l(y)} \right)_{\phi=\phi^0} \right] \right\}_{\varphi=0}, \quad (3.32)$$

In the above the second derivative of the effective action (3.14) at the order ϕ^2 turns out to be:

$$\begin{aligned} \frac{\delta^2 S_{\text{eff}}^B[\phi]}{\delta \phi_i(x) \delta \phi_j(y)} &= \delta_{ij} G_\pi^{0^{-1}}(x-y) + \text{Tr}(\Gamma_i \Gamma_j) \Pi^0(x, y) \\ &+ \sum_k \int du \left[\text{Tr}(\Gamma_i \Gamma_j \Gamma_k) \Pi^0(x, y, u) + \text{Tr}(\Gamma_j \Gamma_i \Gamma_k) \Pi^0(y, x, u) \right] \phi_k(u) \\ &+ \sum_{k,l} \int du dv \left[\text{Tr}(\Gamma_i \Gamma_j \Gamma_k \Gamma_l) \Pi^0(x, y, u, v) + \text{Tr}(\Gamma_j \Gamma_i \Gamma_k \Gamma_l) \Pi^0(y, x, u, v) \right. \\ &\quad \left. + \text{Tr}(\Gamma_i \Gamma_l \Gamma_j \Gamma_k) \Pi^0(x, v, y, u) \right] \phi_k(u) \phi_l(v). \end{aligned} \quad (3.33)$$

The second term in the r.h.s. of eq. (3.33) does not affect the calculation of eq. (3.32). By substituting (3.20) in the equation of motion (3.19), from the terms of order φ^2 we get the following B_{ijk} functions:

$$\begin{aligned} B_{ijk}(x, y, z) &= 2 \text{Tr}(\Gamma_i \Gamma_j \Gamma_k) \int du dv dt \Pi^0(u, v, t) \\ &\times G_\pi^{\text{ring}}(x-u) \left(G_\pi^{0^{-1}} \right) (v-y) \left(G_\pi^{\text{ring}} G_\pi^{0^{-1}} \right) (t-z). \end{aligned} \quad (3.34)$$

Now we have to calculate the logarithm in eq. (3.32) up to second order in φ . We can multiply the generating functional (3.31) by the factor $(\det G_\pi^0)^{-1/2}$, inessential in the calculation of the polarization propagator (this corresponds to multiply eq. (3.33) by G_π^0). Then, after calculating eq. (3.33) for $\phi = \phi^0$, with ϕ^0 given by the eqs. (3.20), (3.24), (3.34), we expand the logarithm up to φ^2 and take the trace to the same order. Finally, the derivation with respect to the external source provides the following total polarization propagator:

$$\Pi_{ij}(x, y) = \delta_{ij} \Pi(x, y), \quad (3.35)$$

with:

$$\begin{aligned}
\Pi(x, y) = & \Pi^{\text{ring}}(x, y) + \sum_{kl} \text{Tr}(\Gamma_k \Gamma_l) \int du dv G_\pi^{\text{ring}}(u - v) \Pi^0(x, u, y, v) \\
& + \sum_{kl} \text{Tr}(\Gamma_k \Gamma_l) \int du dv G_\pi^{\text{ring}}(u - v) [\Pi^0(x, u, v, y) + \Pi^0(x, y, v, u)] \\
& + \int du dv dw ds G_\pi^{\text{ring}}(u - w) G_\pi^{\text{ring}}(v - s) \Pi^0(x, u, v) \\
& \times \sum_{klmn} [\text{Tr}(\Gamma_k \Gamma_l \Gamma_m \Gamma_n) \Pi^0(y, w, s) + \text{Tr}(\Gamma_k \Gamma_l \Gamma_n \Gamma_m) \Pi^0(y, s, w)]. \tag{3.36}
\end{aligned}$$

We remind that the second derivative, with respect to the external source, of $S_{\text{eff}}^B[\phi^{\text{ring}}]$ and $S_{\text{eff}}^B[\phi^0]$, with $\phi^{\text{ring}}[\phi^0]$ given by eq. (3.25) [eqs. (3.20), (3.24), (3.34)], gives the same result (the ring polarization propagator) when evaluated ad $\varphi = 0$.

The Feynman diagrams corresponding to eq. (3.36) are depicted in fig. 4. Diagram (a) represents the Lindhard function $\Pi^0(x, y)$, which is the first term of $\Pi^{\text{ring}}(x, y)$. In (b) we have an exchange diagram (the dashed lines represent ring-dressed pion propagators); (c) and (d) are self-energy diagrams, while in (e) and (f) we show the correlation diagrams of our approximation. The approximation scheme we have developed is also referred to as bosonic loop expansion (BLE). The practical rule to classify the Feynman diagrams according to their order in the BLE is to reduce to a point all its fermionic lines and to count the number of bosonic loops left out. In our case the diagrams (b)-(f) of fig. 4 reduce to a one-boson-loop. Diagrams (b), (c), (d) can be represented by the loop (A) of fig. 5, while (e), (f) correspond to the loop (B).

When we include in the model the excitation of barionic resonances, then we have to replace the fermionic field with multiplets. The topology of the diagrams remains the same as in fig. 4 but, introducing for example the Δ resonance, each fermionic line stands for a nucleon or for a Δ , taking care of isospin conservation. One thus obtain 15 exchange, 30 self-energy and 98 correlation diagrams (see ref. [6] for the whole diagrammology).

Moreover, since this expansion is characterized by the topology of the diagrams, we can include in the model additional mesonic degrees of freedom together with phenomenological short range correlations. In particular, the extension to other spin-isospin channels simply amounts to change the definition of the Γ_i and the same occurs for the non-relativistic reduction of the theory. Accordingly, for the non-relativistic pion exchange Γ_i becomes $(\boldsymbol{\sigma} \cdot \mathbf{q})\tau_i$, for the ρ exchange it reads $(\boldsymbol{\sigma} \times \mathbf{q})_k \tau_i$, k being a spatial index, and for the ω exchange $\Gamma_i = (\boldsymbol{\sigma} \times \mathbf{q})_i$. The exchange of ω -mesons is taken into account only inside the one-boson-loop diagrams (b)-(f) of fig. 4, but not in the mesonic lines stemming from the Λ decay vertex, where the exchanged meson has to be an isovector (π and ρ). Beyond π , ρ and ω mesons, the present approach also contains (partly) the exchange of the scalar-isoscalar σ meson: as in the language of the Bonn potential [14], the latter is described through box diagrams (contained in the correlation diagrams of fig. 4), namely by the exchange of two pions with the simultaneous excitation of one or two of the intermediate nucleons to a Δ .

A further difficulty arises if we start from a potential theory, instead of one containing bosons as true degrees of freedom. This disease is however easily overcome by means of a

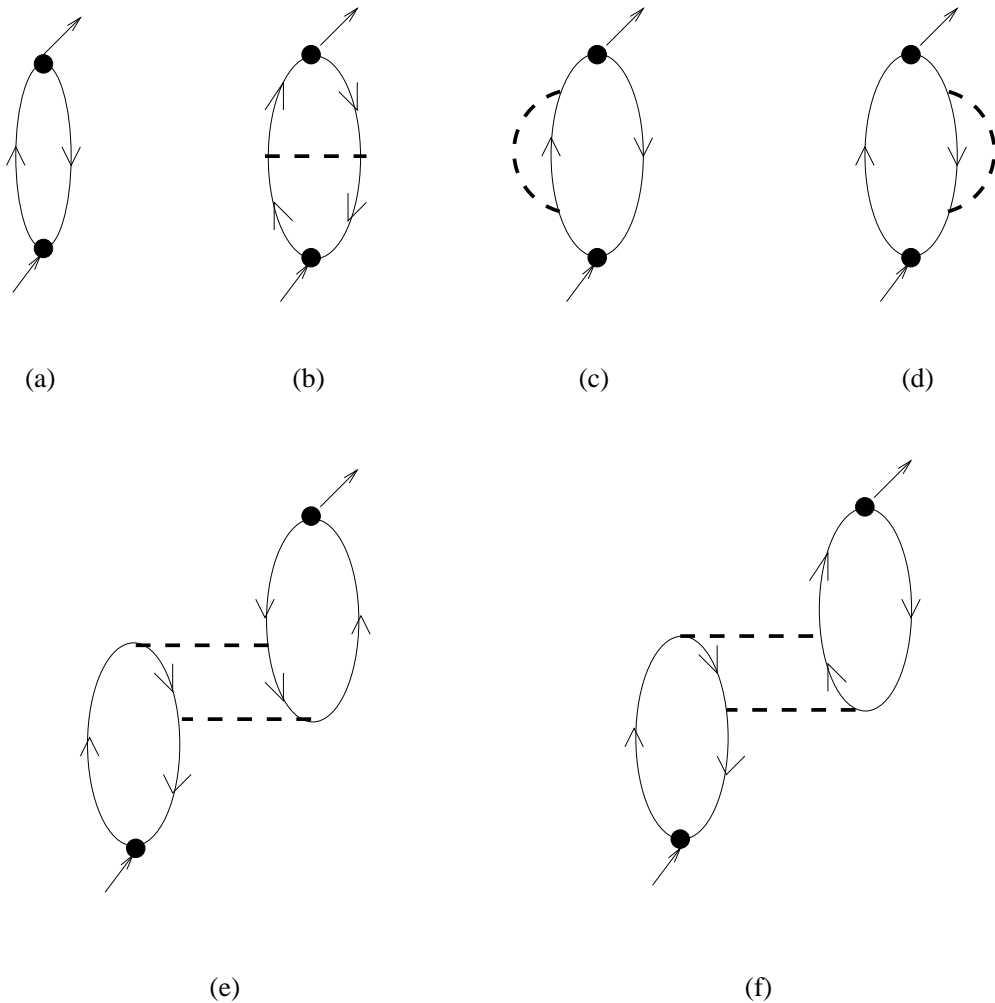


FIG. 4. Feynman diagrams for the polarization propagator of eq. (3.36): (a) particle-hole; (b) exchange; (c) and (d) self-energy-type; (e) and (f) correlation diagrams. Only the first contribution to the p - h ring expansion has been drawn. The dashed line represent ring-dressed pion propagators.

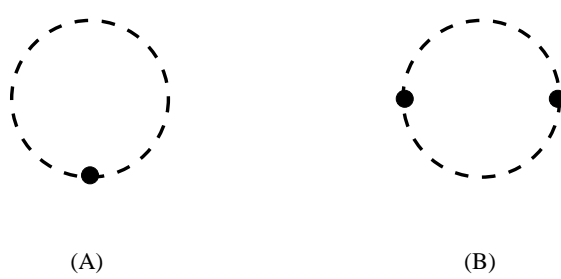


FIG. 5. First order diagrams in the bosonic loop expansion. Diagrams (b), (c), (d) of fig. 4 reduce to diagram (A), while (e), (f) to (B).

Hubbard-Stratonovitch transformation, which enables us to substitute a potential with an interaction of the nucleons with a suitably introduced auxiliary field. For a scalar-isoscalar potential V the relevant identity reads:

$$\exp \left\{ \frac{i}{2} \int dx dy \bar{\psi}(x) \psi(x) V(x-y) \bar{\psi}(y) \psi(y) \right\} = \sqrt{\det V} \int \mathcal{D}[\sigma] \exp \left\{ \frac{i}{2} \int dx dy \sigma(x) V^{-1}(x-y) \sigma(y) + i \int dx \bar{\psi}(x) \psi(x) \sigma(x) \right\}, \quad (3.37)$$

where σ is the auxiliary field. Clearly, the previous derivation will remain valid, providing one substitutes the inverse propagator of the auxiliary field with the inverse potential in the “free” part of the action.

Finally, a relevant point for the feasibility of the calculations is that all fermion loops in fig. 4 can be evaluated analytically [15,16], so that each diagram reduces to a 3-dimensional (numerical) integral.

In particular, the formalism can be applied to evaluate both the longitudinal and the transverse functions $U_{L,T}$ of eq. (2.16), which are required in eqs. (2.7), (2.8). In the approximation of fig. 4 we have to replace eq. (2.8) with:

$$\begin{aligned} \alpha(q) = & \left\{ S^2 + \frac{P^2}{m_\pi^2} \mathbf{q}^2 \right\} F_\pi^2(q) G_\pi^0(q) + \frac{\tilde{S}^2(q) U_1(q)}{1 - V_L(q) U_1(q)} \\ & + \frac{\tilde{P}_L^2(q) U_1(q)}{1 - V_L(q) U_1(q)} + \frac{\tilde{P}_T^2(q) U_1(q)}{1 - V_T(q) U_1(q)} \\ & + [\tilde{S}^2(q) + \tilde{P}_L^2(q)] U_{2,L}(q) + \tilde{P}_T^2(q) U_{2,T}(q), \end{aligned} \quad (3.38)$$

where

$$U_1 = U^{ph} + U^{\Delta h}, \quad (3.39)$$

and $U_{2,L}$, $U_{2,T}$ are evaluated from diagrams (b)-(f) of fig. 4 (taking into account the Δ excitation as well) using the standard Feynman rules. The normalization of these functions is such that $U^{ph}(x, y) = 4\Pi^0(x, y)$, with Π^0 given by eq. (3.16).

IV. RESULTS AND DISCUSSION

In the present work the evaluation of the hypernuclear decays is performed in nuclear matter. However, in order to compare with experimental data on finite (real) nuclei, we employ different Fermi momenta, which are fixed on the following basis. In local density approximation the “local” Fermi momentum $k_F^A(r)$ is related to the nuclear density:

$$\rho_A(r) = \frac{\rho_0(A)}{1 + e^{[r - R(A)]/a}}, \quad \rho_0(A) = \frac{A}{\frac{4}{3}\pi R^3(A) \{1 + [\frac{\pi a}{R(A)}]^2\}} \quad (4.1)$$

($a = 0.54$ fm, $R(A) = 1.12A^{1/3} - 0.86A^{-1/3}$ fm), by the equation:

TABLE I. Average Fermi momenta.

	Γ_{NM}^{exp}	$\langle k_F \rangle$ eq. (4.3) (fm $^{-1}$)	$\langle k_F \rangle$ eq. (4.4) (fm $^{-1}$)
Medium-Light: $^{11}_{\Lambda}\text{B}$ - $^{12}_{\Lambda}\text{C}$	0.94 \div 1.07 [17,18]	0.95	1.08
Medium : $^{28}_{\Lambda}\text{Si}$ - $^{56}_{\Lambda}\text{Fe}$	1.20 \div 1.30 [19]	\simeq 1.1	\simeq 1.2
Heavy: $^{209}_{\Lambda}\text{Bi}$ - $^{238}_{\Lambda}\text{U}$	1.45 \div 1.70 [20-22]	1.21	1.36

$$k_F^A(r) = \left[\frac{3}{2} \pi^2 \rho_A(r) \right]^{1/3}. \quad (4.2)$$

For the present purpose, an average, *fixed* Fermi momentum can be obtained by weighting each local k_F with the density itself:

$$\langle k_F \rangle_A = \frac{1}{A} \int d\mathbf{r} k_F^A(r) \rho_A(r). \quad (4.3)$$

Alternatively (and more realistically) the average Fermi momentum should be determined by the probability density of the Λ inside the nucleus, according to the following definition:

$$\langle k_F \rangle_A = \int d\mathbf{r} k_F^A(r) |\psi_\Lambda(\mathbf{r})|^2, \quad (4.4)$$

ψ_Λ being the Λ wave function. We have calculated the latter from a Wood-Saxon potential with thickness $a = 0.6$ fm and radius and depth which reproduce the measured s and p Λ -levels [1]. Since the Λ wave function is preferably located in the interior of the nucleus (in fact, the hyperon occupies the $1s$ level), we expect larger $\langle k_F \rangle$ values from the prescription (4.4) than from (4.3).

We classify the hypernuclei for which are available experimental data on the non-mesonic decay rate into three mass regions (medium-light: $A \simeq 10$; medium: $A \simeq 30 \div 60$; and heavy hypernuclei: $A \simeq 200$), as shown in table I. The experimental bands include values of the non-mesonic widths which are compatible with all the quoted experiments. In the third and fourth columns we report the corresponding $\langle k_F \rangle$, as calculated with eqs. (4.3) and (4.4), respectively. Accordingly, in the calculations of the decay width we use $k_F = 1.1$ fm $^{-1}$ for medium-light, $k_F = 1.2$ fm $^{-1}$ for medium and $k_F = 1.36$ fm $^{-1}$ for heavy hypernuclei.

Before discussing the results, we list here the parameters which enter the calculation of the hypernuclear width. We point out that their values (with the exception of the Landau parameters g' and g'_Λ , which will be discussed separately) have not been taken as free parameters. Instead, we kept them fixed on the basis of the existing phenomenology (for example in the analysis of the quasi-elastic electron-nucleus scattering, of the spin-isospin nuclear response functions, etc).

- The correlation momentum is set to $q_c = 0.78$ GeV;

- The cut-offs in the pion, ρ and ω form factors are: $\Lambda_{\pi NN} = 1.3$ GeV, $\Lambda_{\pi N\Delta} = \Lambda_{\pi\Delta\Delta} = 1$ GeV, $\Lambda_{\rho NN} = \Lambda_{\rho N\Delta} = \Lambda_{\rho\Delta\Delta} = 2.5$ GeV, $\Lambda_{\omega NN} = \Lambda_{\omega N\Delta} = \Lambda_{\omega\Delta\Delta} = 1$ GeV;
- The pion coupling constants are: $f_{\pi NN}^2/4\pi = 0.08$, $f_{\pi N\Delta}^2/4\pi = 0.32$, $f_{\pi\Delta\Delta}^2/4\pi = 0.016$;
- The rho coupling constants are (see eq. (2.14)): $C_{\rho NN} = C_{\rho N\Delta} = C_{\rho\Delta\Delta} = 2.3$;
- The ω coupling constants are: $C_{\omega NN} = C_{\omega N\Delta} = 1.5$ (renormalized values);
- Finally, the difference between the nucleon and Λ binding energies, which enter eq. (2.7) as $\Delta V = V_\Lambda - V_N$, has been fixed, for the heaviest nuclei ($k_F = 1.36$ fm $^{-1}$), from the corresponding depths of the binding potential ($V_N = -55$ MeV, $V_\Lambda = -32$ MeV). Then, by assuming that ΔV is roughly proportional to the density, we obtain $\Delta V = 18$ MeV at $k_F = 1.2$ fm $^{-1}$ and $\Delta V = 12$ MeV at $k_F = 1.1$ fm $^{-1}$. It is worth pointing out, however, that the resulting widths are only weakly affected by the precise value of ΔV (a change of 5 MeV in ΔV would result in a 3% variation in the decay rates).

The numerical evaluation of the first order contributions in the BLE [diagrams (b)-(f) in fig. 4] presents a serious problem when the mesons (π , ρ and ω in our case) are dynamic. The pionic branch in RPA is coupled to the particle-hole mode. By using non-relativistic kinematics for the nucleons, the relativistic pionic branch enters the particle-hole continuum for a momentum of about 1.6 GeV. This fact generates large oscillations in the calculation of the one-loop diagrams (where the momentum of the mesons is integrated out), which are absolutely unphysical and unavoidable from the numerical point of view. To prevent this mishap, we are forced to use static mesons in the evaluation of the one-boson-loop contributions. In all the mesonic lines of fig. 2 which are “external” to the bosonic loop we can use, on the contrary, the correct dynamical prescription, the relevant momenta being limited to about 0.6 GeV.

An important ingredient in the calculation of the Λ decay rates is the short range part of the NN and ΛN interactions: in fact, in the non-mesonic processes the exchanged momentum is very large (about 400 MeV). We parametrize these short range correlation with the functions reported in the appendix of ref. [1]. The zero energy and momentum limits of these correlations, g' and g'_Λ (which we call, for historical reasons, Landau parameters), are considered as *free parameters*. No experimental constraints are available on g'_Λ , while in the framework of the ring approximation (namely by neglecting the $2p$ - $2h$ states in the Λ self-energy), realistic values of g' lie in the range $0.6 \div 0.7$ [23]. However, in the present context g' correlates not only p - h pairs, but also p - h with $2p$ - $2h$ states and besides, in some diagrams [for instance (d) and (e) of fig. 2], two consecutive g' are connected to the same fermionic line, introducing some double counting, namely a renormalization of g' . In the picture of figures 2 and 4 the Λ self-energy acquires an energy and momentum behaviour which cannot be explained and simulated on the basis of the simple ring approximation. Therefore, the physical meaning of the Landau parameters is different in our scheme with

TABLE II. g' values compatible with the experiments.

	1-loop	ring
$k_F = 1.1 \text{ fm}^{-1}$	$\gtrsim 0.75$	$0.45 \div 0.65$
$k_F = 1.2 \text{ fm}^{-1}$	$0.75 \div 0.90$	$0.55 \div 0.65$
$k_F = 1.36 \text{ fm}^{-1}$	$0.70 \div 1.00$	$0.65 \div 0.75$

respect to the customary phenomenology, hence in the present paper we will use g' as free parameters, to be fixed in order to reproduce the experimental hypernuclear decay rates.

As discussed in ref. [1], for fixed g' the non-mesonic width (the total width in nuclear matter, where $\Gamma_M = 0$) has a minimum as a function of g'_Λ , which is almost independent of the value of g' . This characteristic does not depend on the set of diagrams taken into account in the calculation, but it is simply due to the interplay between the longitudinal and transverse parts of the p -wave $\Lambda N \rightarrow NN$ potential [\tilde{P}_L and \tilde{P}_T functions of eqs. (2.8), (3.38)]. In the present calculation the minimum is obtained, again, for $g'_\Lambda \simeq 0.4$.

Fixing $g'_\Lambda = 0.4$, in ring approximation we can reproduce the experimental decay rates by using g' values which are compatible with the existing literature. In figure 6 we show, as a function of g' (for $g'_\Lambda = 0.4$), the calculated non-mesonic decay widths (in unit of the free Λ width) for the three mass regions of table I. The thick solid curves refer to the one-boson-loop approximation of eq. (3.38) and fig. 4, while the dot-dashed curves are obtained through an RPA iteration of both the particle-hole and the one-boson-loop diagrams, namely by using eq. (2.8). However, we remind that only the former approximation has a theoretically founded basis, in line with the scheme introduced in sec. III: indeed, the present RPA calculation has the tendency to overestimate, in the acceptable range of g' values, the experimental non-mesonic widths. The dashed lines represent the pure ring approximation. The calculation is compatible with the experimental bands for the g' values reported in table II. As we have already noticed, the intervals corresponding to the ring calculation are in agreement with the phenomenology of other processes, like the (e, e') quasi-elastic scattering. However, only the full calculation (column 1-loop) allows for a good description (with the same g' values) of the rates in the whole range of k_F considered here. In fig. 7 we see the dependence of the non-mesonic widths on the Fermi momentum. The solid lines correspond to the one-loop approximation, with $g' = 0.7, 0.8, 0.9$ from the top to the bottom, while the dashed lines refer to the ring approximation, with $g' = 0.5, 0.6, 0.7$ (again from the top to the bottom). We can then conclude that for the one-loop calculation the best choice of the Landau parameters is the following:

$$g' = 0.8, \quad g'_\Lambda = 0.4. \quad (4.5)$$

This parametrization is the same which was employed in a different theoretical framework [1] to reproduce the experimental decay rates in the range $^{12}\Lambda\text{C} - ^{238}\Lambda\text{Pb}$. However, we must

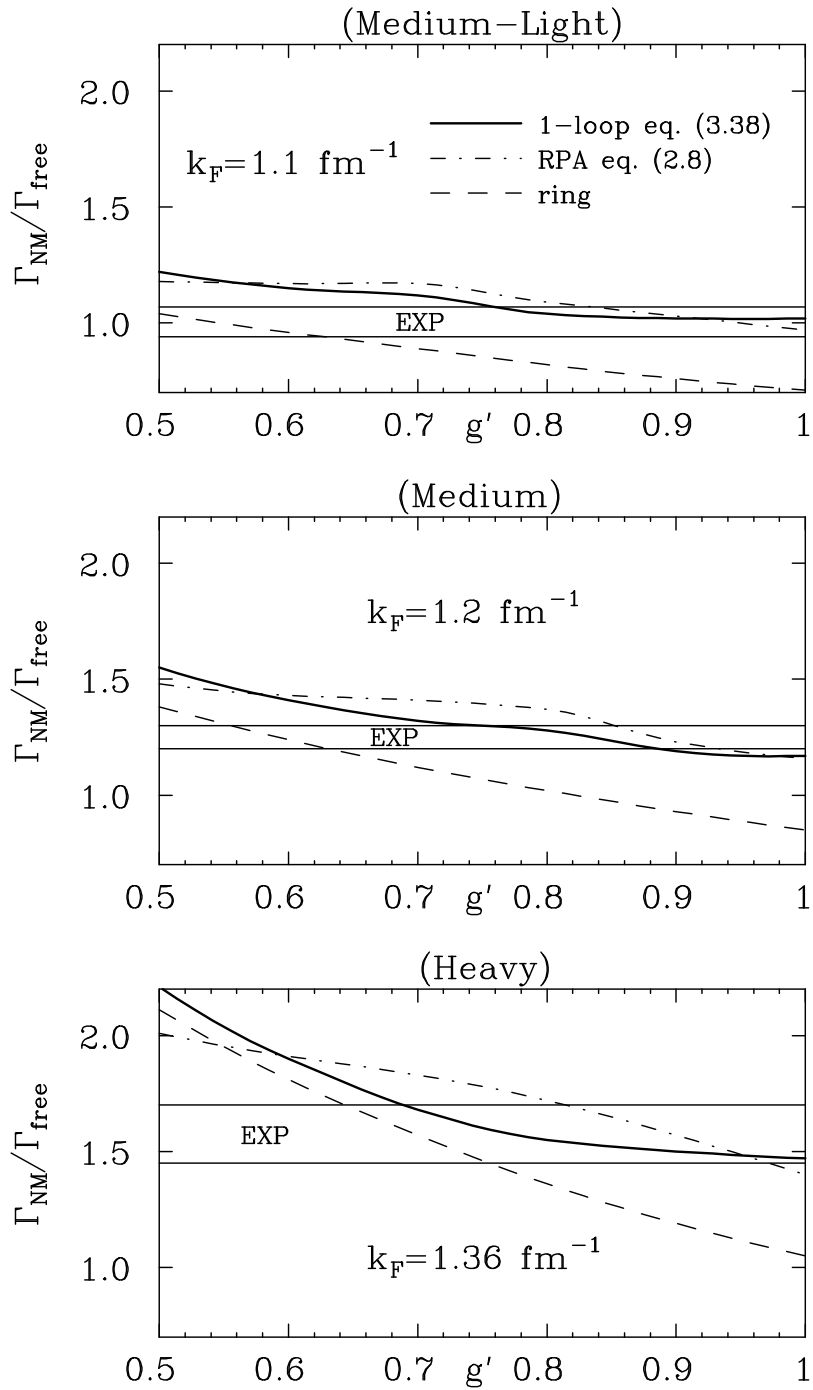


FIG. 6. Dependence of the non-mesonic width on the Landau parameter g' , for $g'_\Lambda = 0.4$. The three plots correspond to the classification of table I. The thick solid curves refer to the one-boson-loop approximation of eq. (3.38), the dot-dashed ones to the RPA calculation of eq. (2.8) and the dashed ones to the ring approximation. The experimental bands of table I lies in between the horizontal solid lines.

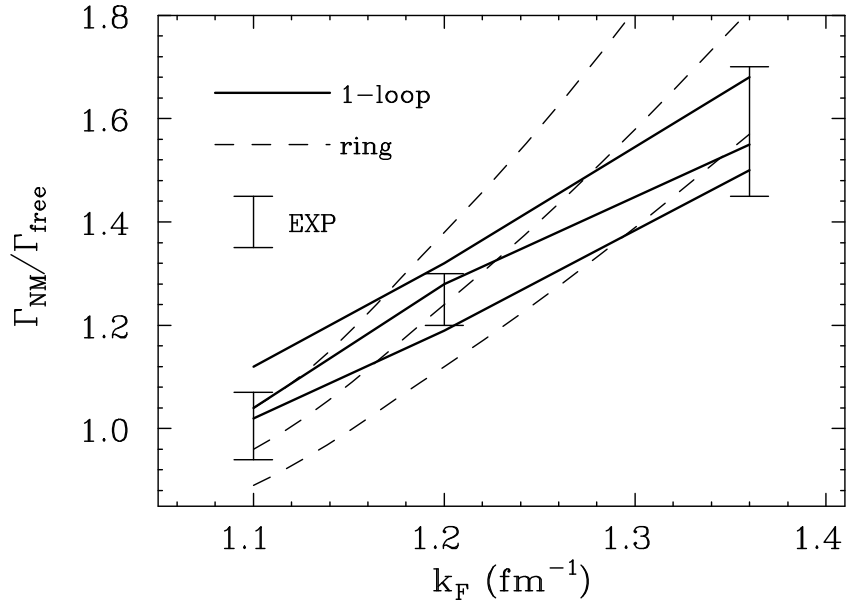


FIG. 7. Dependence of the non-mesonic width on the Fermi momentum. The solid curves refer to the one-boson-loop approximation (with $g' = 0.7, 0.8, 0.9$ from the top to the bottom), while the dashed lines refer to the ring approximation ($g' = 0.5, 0.6, 0.7$). The experimental data are also shown.

point out that in the previous calculation the $2p$ - $2h$ contributions in the Λ self-energy were evaluated by using a phenomenological parametrization of the pion-nucleus optical potential, also accounting for the available phase space for the $2p$ - $2h$ states. The role played by the Landau parameters is different in the two approaches. In the present paper we have microscopically evaluated all the relevant diagrams which contribute at the one-boson-loop level; however, due to the very long computing times, we cannot implement the calculation for finite nuclei through the local density approximation used in [1].

The fairly large value of g' , which we adopt in order to reproduce the Λ widths in the one-boson-loop approximation, deserves some comment. Indeed, beside the above mentioned phenomenology within the framework of ring approximation, which favoured values of g' between 0.6 and 0.7, previous calculations of the (e, e') inclusive longitudinal response function within the one-boson-loop approximation [6] employed a rather small value ($g' = 0.35$) of this parameter. We remind that the longitudinal response only concerns the scalar-isoscalar and scalar-isovector channels: hence neither the π or ρ mesons nor g' enter the particle-hole interaction lines external to the one bosonic loop diagrams. Therefore, in ref. [6] g' was employed *only* in conjunction with static mesons. In order to understand the influence in the present calculation of the dynamical (external) pion propagation, we show in figure 8 the results of a completely static calculation (also the “external” mesonic lines are static). The non-mesonic widths we obtain in this case are smaller than in figure 6 and the experimental

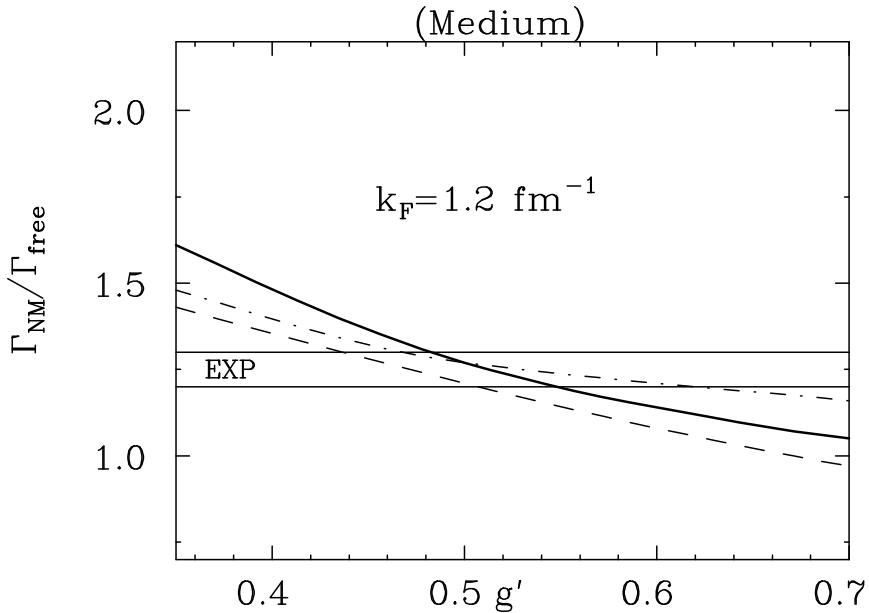


FIG. 8. Dependence of the non-mesonic width on the Landau parameter g' , for $g'_\Lambda = 0.4$ and $k_F = 1.2 \text{ fm}^{-1}$ in the static limit. The various curves have the same meaning as in fig. 6.

band is generally reproduced by using smaller g' values: typically $g' = 0.5$ in the one-loop approximation. This outcome somehow reconciles the parametrization of the short range correlations used in the evaluation of the hypernuclear decay rates with the one of ref. [6] for the nuclear responses in the inclusive electron scattering.

In table III we show the comparison between the one-boson-loop approximation (OBL) and the phenomenological model (PM) of ref. [1] at fixed k_F . The calculations have been carried out in both cases with $g' = 0.8$ and $g'_\Lambda = 0.4$. For technical reasons, the OBL calculation does not allow to precisely identify the partial ratios Γ_1 and Γ_2 which contribute to the total $\Gamma_{NM} = \Gamma_1 + \Gamma_2$. In fact, we cannot separate in the imaginary parts of the diagrams (b)-(f) of fig. 4 the contributions coming from cuts on p - h and $2p$ - $2h$ states, and hence the partial width (Γ_2) stemming from the two-nucleon induced decay. The values listed in the table for Γ_2^{OBL} have been obtained from the total imaginary part of the diagrams 4(b)-4(f) [namely from the last two terms in the r.h.s. of eq. (3.38)]. In this approximation, $\Gamma_1^{\text{OBL}} = \Gamma_{\text{ring}}$ [second, third and fourth terms in the r.h.s. of eq. (3.38)]. As a matter of fact, one would expect that Γ_2 increases with k_F (and this is the case for the PM calculation), but the OBL results do not follow this statement. From table III and from the study of the g' -dependence of Γ_2^{OBL} , the only conclusion we can draw on the two-body induced process in OBL approximation is that for $1.1 \text{ fm}^{-1} \lesssim k_F \lesssim 1.36 \text{ fm}^{-1}$ and $0.5 \lesssim g' \lesssim 1$, $\Gamma_2/\Gamma_{\text{free}} = 0.1 \div 0.3$.

TABLE III. Comparison between the one-boson-loop approximation (OBL) and the phenomenological model (PM) of ref. [1] for $g' = 0.8$, $g'_\Lambda = 0.4$. The decay rates are in unit of the free Λ width.

	$k_F = 1.1 \text{ fm}^{-1}$		$k_F = 1.2 \text{ fm}^{-1}$		$k_F = 1.36 \text{ fm}^{-1}$	
	OBL	PM	OBL	PM	OBL	PM
Γ_1	0.82	0.81	1.02	1.00	1.36	1.33
Γ_2	0.22	0.13	0.26	0.18	0.19	0.26
Γ_{NM}	1.04	0.94	1.28	1.19	1.55	1.59

V. CONCLUSIONS

The Λ non-mesonic decay widths have been evaluated in nuclear matter within the polarization propagator method. The Feynman diagrams contributing to the Λ self-energy have been classified, via a functional approach, by the first order approximation of the bosonic loop expansion. In this scheme, the two-body induced decay $\Lambda NN \rightarrow NNN$ is taken into account for the first time from a fully microscopic point of view.

In order to compare the calculation with the available experimental data, we have employed different “average” Fermi momenta for the following three mass regions: medium-light ($A \simeq 10$); medium ($A \simeq 30 \div 60$); and heavy hypernuclei ($A \simeq 200$).

The only free parameters of our model are g' and g'_Λ , which incorporate the NN and ΛN short range interactions, respectively. We have fixed these Landau parameters in order to reproduce the observed decay widths, and, in the one-boson-loop approximation, the best choice has turned out to be $g' = 0.8$, $g'_\Lambda = 0.4$. The agreement between the experimental widths and the theoretical evaluation is of the same quality as in ref. [1]; interestingly, the same values of g' and g'_Λ give the best fit to the data in both approaches. However, we point out that the role of these Landau parameters is slightly different in the two cases. One difference, with respect to ref. [1], in the role played by g' and g'_Λ can be understood by comparing equations (2.8) and (3.38): clearly, in the former (employed in ref. [1]) the short range correlations have a major influence in renormalizing the full polarization propagator $U_{L,T}$, while in the latter (used in the present calculation) the RPA renormalization only affects the Lindhard function U_1 . Moreover, in the present calculation g' comes about together with static mesons (because of the discussed computational problems) in the lines “internal” to the bosonic loops and together with dynamical mesons in the lines “external” to the bosonic loops, while in [1] all mesonic lines are dynamical. We also note that, by introducing a completely static description, the experimental data are reproduced with smaller g' values ($\simeq 0.5$). This finding is in fairly good agreement with the parametrization introduced in ref. [6] for the BLE calculation of the nuclear response functions in the inclusive electron scattering, where g' only correlates static mesons, as explained in the previous section.

Finally, while the estimated Γ_1^{OBL} only contains one-body induced decays (in ring approximation), contributions to the total width stemming from this channel are also embodied in Γ_2^{OBL} , but cannot be explicitly separated from the truly two-body induced ones. On the basis of reasonable estimates, the two-body stimulated decay is found to be sizeable, ($\Gamma_2/\Gamma_{\text{free}} = 0.1 \div 0.3$ for the whole hypernuclear mass spectrum studied), with values comparable with the results of ref. [1].

In conclusion, the present calculation satisfactorily reproduces the non-mesonic decay widths for $A \gtrsim 10$ within a fully microscopic approach at fixed, average density, taking into account both one-body and two-body induced processes.

ACKNOWLEDGMENTS

We acknowledge financial support from the MURST.

REFERENCES

- [1] W. M. Alberico, A. De Pace, G. Garbarino and A. Ramos, [nucl-th/9902023](#).
- [2] E. Oset and J. Nieves, *Phys. Rev.* **C47** (1993) 1478.
- [3] K. Itonaga, T. Ueda and T. Motoba, *Nucl. Phys.* **A585** (1995) 331c.
- [4] J. W. Negele, *Rev. Mod. Phys.* **54** (1982) 813.
- [5] W. M. Alberico, R. Cenni, A. Molinari and P. Saracco, *Ann. Phys.* **174** (1987) 131.
- [6] R. Cenni, F. Conte and P. Saracco, *Nucl. Phys.* **A623** (1997) 391.
- [7] E. Oset and L. L. Salcedo, *Nucl. Phys.* **A443** (1985) 704.
- [8] A. Ramos, E. Oset and L. L. Salcedo, *Phys. Rev.* **C50** (1995) 2314.
- [9] A. Parreño, A. Ramos, C. Bennhold and K. Maltman, *Phys. Lett.* **B 435** (1998) 1.
- [10] A. Parreño, A. Ramos and C. Bennhold, *Phys. Rev.* **C56** (1997) 339.
- [11] J. F. Dubach, G. B. Feldman, B. R. Holstein and L. de la Torre, *Ann. Phys.* **249** (1996) 146.
- [12] A. L. Fetter and J. D. Walecka, *Quantum Theory of Many Particle Systems* (McGraw-Hill, New York, 1971).
- [13] E. Oset, P. Fernández de Córdoba, L. L. Salcedo and R. Brockmann, *Phys. Rep.* **188** (1990) 79.
- [14] R. Machleidt, K. Holinde, and Ch. Elster, *Phys. Rep.* **149** (1987) 1.
- [15] R. Cenni and P. Saracco, *Nucl. Phys.* **A487** (1988) 279.
- [16] R. Cenni, F. Conte, A. Cornacchia and P. Saracco, *Rivista del Nuovo Cimento* vol. 15 n. 12 (1992).
- [17] J. J. Szymanski et al., *Phys. Rev.* **C43** (1991) 849.
- [18] H. Noumi et al., *Phys. Rev.* **C52** (1995) 2936.
- [19] H. C. Bhang et al., *Nucl. Phys.* **A639** (1998) 269c.
- [20] P. Kulessa et al., *Phys. Lett.* **B427** (1998) 403.
- [21] T. A. Armstrong et al., *Phys. Rev.* **C47** (1993) 1957.
- [22] H. Ohm et al., *Nucl. Phys.* **A629** (1998) 416c.
- [23] E. Oset, H. Toki and W. Weise, *Phys. Rep.* **83** (1982) 281.